Tissue Engineering III: Cell - Surface Interactions for Tissue Culture

Bearbeitet von
Cornelia Kasper, Frank Witte, Ralf Pörtner

1. Auflage 2012. Buch. xiv, 342 S. Hardcover
ISBN 978 3 642 28281 2
Format (B x L): 15,5 x 23,5 cm
Gewicht: 695 g

Adv Biochem Engin/Biotechnol (2012) 126: 33–66
DOI: 10.1007/10_2011_112

Published Online: 12 October 2011

Studying Cell–Surface Interactions In Vitro: A Survey of Experimental Approaches and Techniques

Stefanie Michaelis, Rudolf Robelek and Joachim Wegener

Abstract A better understanding of the interactions of animal (or human) cells with in vitro surfaces is the key to the successful development, improvement and optimization of biomaterials for biomedical or biotechnological purposes. State-of-the-art experimental approaches and techniques are a prerequisite for further and deeper insights into the mechanisms and processes involved in cell–surface adhesion. This chapter provides a brief but not complete survey of optical, mechanical, electrochemical and acoustic devices that are currently used to study the structural and functional properties of the cell–surface junction. Each technique is introduced with respect to the underlying principles before example data are discussed. At the end of the chapter all techniques are compared in terms of their strengths, limitations and technical requirements.

Keywords Cell–surface interactions · Cell–surface junction · Cell adhesion · Cell migration · Cell spreading · Electric cell–substrate impedance sensing · Micromotion · Surface plasmon resonance · Quartz crystal microbalance

Abbreviations

ECIS	Electric Cell–Substrate Impedance Sensing
ECM	Extracellular Matrix
RICM	Reflection Interference Contrast Microscopy
SPR	Surface Plasmon Resonance
TIRF	Total Internal Reflection Fluorescence
TIRAF	Total Internal Reflection Aqueous Fluorescence
QCM	Quartz Crystal Microbalance

S. Michaelis · R. Robelek · J. Wegener (✉)
Institut für Analytische Chemie, Chemo- und Biosensorik,
Universität Regensburg, Universitätsstr. 31,
93053 Regensburg Germany
e-mail: Joachim.Wegener@chemie.uni-regensburg.de

Contents

1 Cell–Surface Interactions from Two Perspectives

Cells interact with their environment in many different ways: (1) they generate and withstand mechanical stress; (2) they secrete and sense individual signal molecules or molecular cocktails; and (3) they can establish and perceive electrical signals. In a multi-cellular organism all of these or just a subset may provide important clues for a cell to differentiate into one specific phenotype with site-specific functionalities that are important for the organism as a whole. The interactions of cells with their extracellular environment mediated by cell-surface receptors are of paramount importance. Besides their mechanical importance for processes like cell migration during development and wound healing, they provide the basis for inside-out and outside-in signaling. The non-cellular extracellular environment, summarized as the extracellular matrix (ECM), is a complex multi-component mixture consisting of (glyco)-proteins, carbohydrates, low-molecular-weight compounds, electrolytes and water [1]. The macromolecules interact with each other forming a two- or three-dimensional fibrous network that plays a crucial role in tissue homeostasis, mechanics and functionality. Thus, from this biological perspective the interactions of cells with biomaterial surfaces within the organism are critically important for both the cell and the organism.

When cells are isolated from the organism and transferred to an in vitro environment for biomedical or biotechnological purposes, they may lose their specific differentiation and functions due to the absence of the three-dimensional tissue architecture and important molecular clues. In order to maintain the cellular phenotype in vitro for research, medical approaches or biotechnology applications it is important to provide a biocompatible environment. Besides the chemical composition of the growth medium, it is the surface of the cell culture vessels that is critical for cell survival and fate. In particular, the in vitro culture of anchorage-dependent cells, which undergo apoptosis unless they can find proper sites for cell adhesion, relies on tailored in vitro surfaces. Thus, from the perspective of biotechnology, there is a strong need to understand, develop and refine the

properties of in vitro surfaces such that growth and differentiation of the cells is not affected—or even guided in a certain direction. There is not, however, one ideal surface that is well-suited for all kinds of cells and for all scenarios. The most appropriate material depends certainly on the cell type and also on the cellular property that the in vitro surface is supposed to support and to foster, such as cell adhesion, proliferation, differentiation, motility and expression of tissue-specific genes, to mention just a few.

Even though some general correlations between the physico-chemical properties of a given surface and its performance as a support for cell adhesion and growth have been established, there is no in-depth understanding of which surface features influence which cellular function. Many more systematic studies need to be done and they all rely on techniques capable of studying the cell–material interface from different perspectives. This chapter summarizes the established and some of the emerging techniques of analyzing the interface between cells and man-made surfaces. They comprise optical, electrochemical and acoustic approaches, which are compared and categorized at the end of the chapter.

2 Hallmarks of Cell Adhesion on In Vitro Surfaces

Cells do not interact directly with the surface of a man-made material but with a pre-adsorbed layer of extracellular biomolecules, mostly proteins from the ECM [1]. As a direct consequence, the adhesiveness of the surface for ECM-proteins is the first prerequisite for cytocompatibility and mainly determines the behavior and compliance of an in vitro surface in a physiological environment. However, when a man-made material is brought in contact with a biological fluid (e.g. blood, lymphatic fluid or cell culture medium), the surface initially encounters water molecules. These bind rapidly to the surface, establishing a water mono- or bi-layer. The specific arrangement of water molecules depends on the surface properties on the atomic level. Highly reactive surfaces lead to the dissociation of H_2O and form a hydroxylated, i.e. OH-terminated surface. Less reactive surfaces can interact with H_2O molecules by hydrogen bonding, leaving the water as intact, undissociated molecules. Surfaces that show either of these behaviors are termed *wetting* or *hydrophilic* surfaces. On the other hand, surfaces with a weak tendency for binding H_2O are termed *non-wetting* or *hydrophobic*. After the formation of this adsorbed water layer (adlayer), which occurs within nanoseconds, hydrated ions such as Cl^- and Na^+ get incorporated. The specific arrangement of these ions and their water shells is strongly influenced by the properties of the surface.

Subsequently, proteins from the biological fluid adsorb to the surface in a complex series of events, including initial adsorption, conformational changes and eventually replacement of smaller proteins by larger ones. In experiments in vitro these proteins originate from the serum-containing culture medium and/or they are synthesized and secreted by the cells themselves. Depending on the properties of the surface, the resulting mixture of proteins on the surface, their conformational

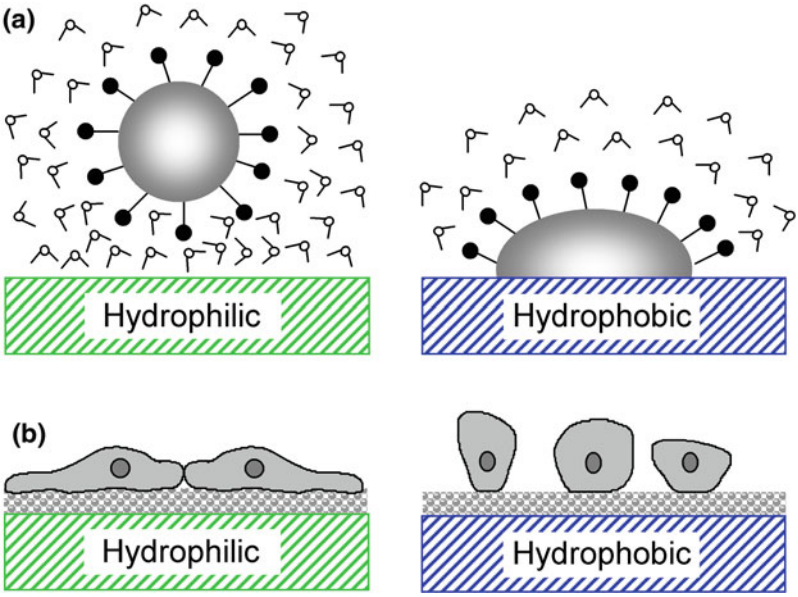

Fig. 1 Hydrophilic or hydrophobic in vitro surfaces in contact with a biological environment. **a** Protein adsorption, **b** cell adhesion (water molecules, polar amino acid side chains)

state and their orientation will be different [2]. Surface wettability is regarded as one of the most important surface parameters governing protein adsorption [3]. A common observation is that hydrophilic and hydrophobic surfaces bind proteins differently, i.e. proteins may adsorb intact or may undergo unfolding to minimize the free energy of the system (Fig.1a). Water-soluble proteins in a physiological environment commonly show a globular shape with a hydrophobic core and hydrophilic and charged amino acid side chains exposed to the solution. Thus, on hydrophilic surfaces protein adsorption occurs through polar and ionic interactions (Fig.1a, left panel). No conformational changes are induced and the proteins bind in their native conformation with intact water shells [4]. This leads to a rather weak, mostly reversible protein adsorption.

On hydrophobic surfaces the proteins are often irreversibly bound due to dehydration of the interface and the associated absence of intervening water shells. Dehydration of both the substrate and the protein surface provides an entropic driving force for the adsorption on hydrophobic surfaces. This leads inevitably to a significant rearrangement of the protein conformation with partial or total unfolding. The hydrophobic amino acids of the protein core are exposed to the substrate surface to allow for hydrophobic interactions with the surface [5]. Most of the polar and charged amino acid residues are oriented towards the aqueous solution (Fig.1a, right panel). The degree of the surface-induced conformational change mirrors the balance between the strength of protein–surface interactions and the internal conformational stability of the protein [6]. The adsorbed protein

layer forms within the first few seconds of contact between the surface and the biological environment and determines the compliance of the surface with subsequent cell attachment and spreading.

After the adsorption of proteins, cell attachment and spreading are initiated by nonspecific interactions between the cells and the protein-decorated surface (Fig. 1b). These comprise electrostatic, electrodynamic, steric and entropic interactions. The first two are predominantly attractive in nature and based on the presence of fixed charges and dipoles on both the cell surface and the substrate surface. On the other hand, close adhesion between cell and surface requires the compression of the glycocalix decorating the cell membrane and the surface-attached protein layer which gives rise to steric and entropic repulsion. Once the balance of nonspecific interactions has provided sufficiently close proximity, specific interactions between cell–surface receptors and the surface immobilized proteins are established and provide mechanically stable substrate anchorage of the cells [7, 8]. The most prominent class of cell-surface receptors involved in cell adhesion and spreading is the integrin family, which will be discussed in more detail in the subsequent section.

Whether or not stable substrate anchorage occurs depends on (1) the expression of integrins with affinity for the extracellular proteins pre-adsorbed on the surface and (2) the composition of the surface attached protein layer and the conformation of the adsorbed proteins. These two conditions eventually determine the fate of cells settling upon an in vitro surface: the cells will start to attach firmly and spread, maximizing their interface with an adhesive surface (Fig.1b, left panel) or they will stay in a rounded morphology, loosely attached and unable to spread, when specific interactions cannot be formed (Fig. 1b, right panel). The latter will drive anchorage-dependent cells towards apoptosis. Generally speaking, while hydrophilic surfaces promote cell adhesion due to their coating with a native protein layer, hydrophobic surfaces covered with a layer of unfolded protein often counteract cell adhesion since specific recognition sequences within the extracellular proteins are not accessible to the cell-surface receptors.

3 Molecular Architecture of Specific Cell–Surface Interactions

The most prominent type of transmembrane receptors responsible for specific cell–substrate interactions are the integrins [9]. Integrins are a family of non-covalently associated, α,β-heterodimeric transmembrane glycoproteins that project from the cell membrane by roughly 20 nm [10]. To date, 24 different integrins have been identified, resulting from different combinations of 18 α- and 8 β-subunits [11].

Both subunits exhibit some structural similarity: each is composed of a long stalk-like extracellular segment with a globular domain at the N-terminus. The N-terminal domains of both subunits combine to form the specific ligand binding site that interacts with ECM proteins in the presence of divalent cations (Mg^{2+} or Ca^{2+}).

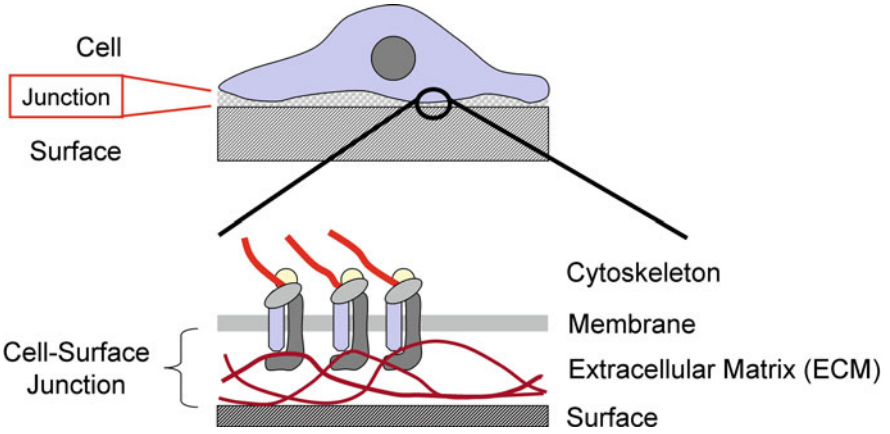

Fig. 2 Contact area between lower cell membrane and substrate surface forming the *cell–surface junction*. Adhesion is provided by cell-surface receptors that specifically bind to components of the ECM pre-adsorbed upon the substrate surface (adapted from [12])

Both subunits share a hydrophobic domain, which spans the cell membrane, and rather small cytosolic C-terminal domains. On the intracellular side, the β-subunit of the integrins is linked to the actin cytoskeleton [13, 14] by means of cytoskeletal adapter proteins (Fig. 2), such as talin, vinculin, α-actinin and paxillin. In contrast to all other integrins, the $\alpha_6\beta_4$ integrin associates with the keratin intermediate filaments (hemi-desmosomes). Thus, integrins interconnect the intracellular protein filaments of the cytoskeleton with the protein filaments of the ECM and serve as a transmembrane bridge between these two macromolecular networks (Fig. 2), providing mechanical stability to the cell–surface junction. The distribution of integrins in the plasma membrane of adherent cells is very often not homogeneous. After ligand binding, they tend to cluster locally, forming so-called focal adhesions or focal contacts [1, 15]. At these adhesion sites, the cells are believed to have the closest distance to the surface.

Depending on their subunit composition, integrins differ significantly with respect to their specificity for different ECM proteins. Molecular recognition and binding of individual ECM proteins are generally mediated by rather short amino acid sequences ($\sim$4 – 10 amino acids) within the primary structure of ECM proteins. The most well-known amino acid sequence involved in integrin recognition is the tetrapeptide binding motif Arg-Gly-Asp-Ser (RGDS), a sequence found in many ECM ligands including the ECM proteins fibronectin and vitronectin [14,16]. Many integrins are multispecific receptors, meaning that they can bind several different ECM proteins as long as these carry a suitable recognition sequence. On the other hand, one particular ECM protein may interact with various integrins by carrying more than one recognition sequence in its primary structure.

Apart from their crucial functional role in cell adhesion and linkage of the cytoskeleton to the ECM [10], integrins act as bi-directional signaling receptors that mediate information transfer across the plasma membrane and thereby

regulate various cellular processes. In *outside-in* signaling ligand binding is transmitted into the cell interior by conformational changes of the receptor carrying information that mediates cell growth, differentiation, proliferation, migration, morphology and survival [1, 13, 17–20]. In addition, integrins transfer signals from the cells to the ECM, a process termed *inside-out* signaling. This process is mainly involved in regulation of integrin conformation, ligand-binding affinity and ECM remodeling [19].

4 Experimental Techniques for Studying Cell–Surface Interactions

The constant improvement in biomaterial synthesis and surface modifications has provided various different synthetic materials that should be tested and screened for their ability to promote cell adhesion and to support or even induce cellular functionalities. A set of experimental approaches has been used in the past to evaluate the cyto-compatibility of a given surface. These established techniques cover a significant range of technical sophistication comprising low and high tech. On the low-tech side, for instance, the number of cells that has adhered to a surface under study within a given time is quantified by simple cell counting upon microscopic examination. For cell proliferation studies, this measurement is repeated at regular intervals. Apart from counting, the amount of cells adhering to a surface under study can be determined by photometry after intracellular uptake of membrane-permeable dyes or other methods of cell staining or biochemical assays. The colorimetric MTT assay is an established in vitro assay for evaluating the cyto-compatibility of biomaterials by measuring the metabolic activity of the cells in contact with the surface. It is based on the intracellular reduction of a colorless tetrazolium salt to colored formazan, which only occurs in metabolically active cells with sufficient supplies of reducing agents ($FADH_2$, NADH). The amount of the colored formazan is proportional to the number of vital cells and can easily be quantified by photometry.

More on the high-tech side are high-resolution microscopic techniques that are capable of imaging the morphology of cells in contact with a surface under study, such as scanning force microscopy (SFM) or scanning electron microscopy (SEM). Both approaches provide detailed images of the upper cell surface with a high spatial resolution. Other microscopic approaches can also be used to image the cells on the surface at different resolutions and contrast.

All the methods mentioned above do not have direct access to the interface between the lower cell membrane and the substrate that the cell is adhered to. We refer to this interface as the *cell–surface junction* (cf. Fig. 2). However, most of the processes important for adhesion, spreading or migration of cells are localized at this particular interface between cell and surface. Thus, all experimental techniques capable of reporting from this hidden area should be very useful for

studying all aspects of cell–substrate adhesion. Moreover, most of the techniques mentioned above are invasive in nature and only provide an endpoint analysis. In order to get insight into the dynamics of cell–surface interactions, non-invasive approaches are required capable of recording the different steps of cell–material encounter with a reasonable time resolution.

In the following paragraphs we will highlight a few techniques and approaches that are particularly valuable for studying the cell–surface interface. Most of the techniques are non-invasive in nature; all of them report directly from the cell–surface junction. They are based on optical, mechanical, electrical or acoustical principles and are grouped accordingly. This survey does not claim completeness but picks the most valuable techniques in the authors' judgment.

4.1 Optical Methods for Studying Cell–Surface Interactions

4.1.1 Reflection Interference Contrast Microscopy

Reflection interference contrast microscopy (RICM) is capable of visualizing the contact area between living cells and a transparent substrate, providing something like the "footprints" of cells rather than their projections. It has been used extensively to study cell adhesion dynamics [21]. In RICM, cells are grown on a glass coverslip which is placed under an inverted microscope and is illuminated from below by monochromatic light using an objective with high illumination numerical aperture (INA). The RICM image results from light that is reflected at interfaces between media of different refractive indices like the glass/liquid and the liquid/cell membrane interfaces. When the incident light hits the transparent substrate at a cell-free area, a fraction of the incident light is reflected at the glass/liquid interface (Fig. 3a). The intensity of the reflected light depends on the difference in the refractive indices of the two adjacent media. Since this difference is more significant for the glass/liquid interface compared to any of the other interfaces of the sample, the reflection is relatively strong, which makes cell-free areas of the sample appear bright in RICM images (Fig. 3b). In cell-covered areas, the incident light is also reflected at the glass/liquid interface but here the reflected light is modulated by interference. The fraction of the incident light passing through the glass/liquid interface is reflected at the liquid/cell membrane interface. Due to the close proximity of these two interfaces (10–200 nm), both reflected light beams are partly coherent and interfere. Thus, the intensity of the reflected light—or the overall brightness of the image in cell-covered areas-depends on the optical path difference of the two reflected light beams. Reflections from interfaces deeper in the sample cannot modify the contrast of RICM images, as the condition of local coherence is not valid for points within the sample that are further away from the surface than approximately 100 nm. Taken together, the brightness of RICM images in cell-covered areas is a function of the distance between the lower cell membrane and the surface [22].

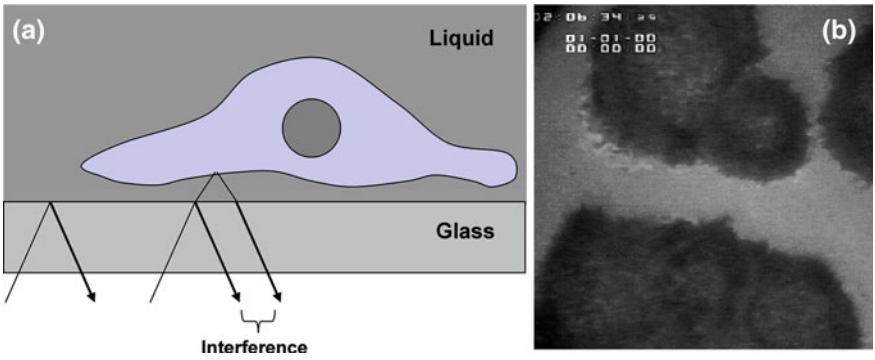

Fig. 3 **a** Image formation in RICM. Light reflected from the glass/liquid interface and the liquid/cell membrane interface is partly coherent and interferes. The image contrast depends on the optical path difference between the two light beams and, thus, the cell–substrate separation distance. **b** Typical RICM image of a cell after attachment and spreading on a glass coverslip

In the corresponding RICM image (Fig. 3b) the contact area of a cell with a substrate appears dark against a homogeneous grey and cell-free background, whereas the intensity of the dark regions themselves depends on the local distance of the lower cell membrane from the substrate surface. Besides providing static information about the cell–surface junction, this technique can also record dynamic processes, such as cell motion, due to its non-invasive nature [23]. However, it is very tricky to extract absolute distances between cell membrane and surface from RICM images, as the refractive indices of the different layers of the sample are very critical parameters during analysis but hard to measure with sufficient precision.

4.1.2 Fluorescence Interference Contrast Microscopy

Another microscopic technique imaging the cell–surface junction is fluorescence interference contrast microscopy (FLIC), which was introduced by Braun and Fromherz in 1997. This technique is capable of quantifying the exact cell–substrate separation distance [24]. Cells are grown on silicon substrates with steps made from silicon dioxide on their surface. The steps have at least four different, known heights ranging between 20 and 200 nm (Fig. 4a). After attachment and spreading of cells on a FLIC substrate, the cell membranes are stained with a lipophilic fluorescent dye and the sample is examined in an upright fluorescence microscope. FLIC microscopy is based on the effect that the fluorescence intensity of the fluorophore in the substrate-facing membrane is modulated by the silicon/silicon dioxide interface which behaves like a mirror.

During illumination, standing waves of the incident light are formed with a node at the silicon surface. Thus, the intensity of fluorophore *excitation* is dependent on the distance between fluorophore (cell membrane) and silicon. The fluorescent light emitted by the fluorophore upon excitation is collected from the objective lens of

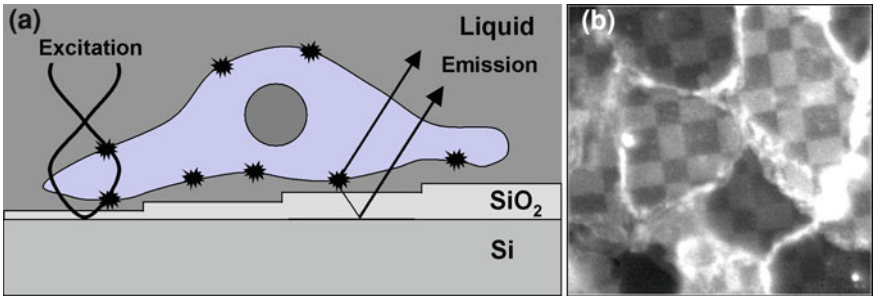

Fig. 4 **a** Schematic illustrating image formation in FLIC microscopy (adapted from [24]). **b** Fluorescence micrograph of a cell grown on a FLIC substrate

the microscope either directly or after reflection at the silicon/silicon dioxide interface. Since both the direct and the reflected fluorescent light are partly coherent, interference occurs so that the intensity of the fluorescence emission is also modulated by the optical path difference between membrane and silicon surface. Taken together, the intensity of fluorophore excitation and the intensity of the resulting fluorescence light are a function of the cell–substrate separation distance. However, the relationship between the relative fluorescence intensity and the distance of the fluorophore to the silicon substrate surface is not unique but a damped periodic function. The four different steps of silicon dioxide, serving as well-defined spacers between the cell membrane and the reflecting silicon surface, are used to provide four data pairs. The four different fluorescence intensities (cp. Fig. 4b) are analyzed using an optical theory, providing a distinct cell–substrate separation distance with unprecedented precision of 1 nm [24, 25]. However, FLIC is not a label-free method and the cells may experience phototoxicity when repeated experiments are performed to follow dynamic processes at the cell–surface junction.

4.1.3 Total Internal Reflection (Aqueous) Fluorescence Microscopy

Total internal reflection fluorescence microscopy (TIRF) [26] and total internal reflection aqueous fluorescence microscopy (TIRAF) [27] are additional microscopic techniques for visualizing the cell–surface junction of living cells as long as they are grown on a transparent substrate. Both TIRF and TIRAF are subsumed under the generic term evanescent field microscopy. In contrast to RICM and similarly to FLIC, either the cell membrane (TIRF) or the incubation fluid (TIRAF) requires fluorescent labeling. The cells under study are grown on a transparent substrate that is illuminated from below with a laser beam. The laser beam is aligned in such a way that it strikes the glass/liquid interface at an angle bigger than or equal to the critical angle of total internal reflection θ_{crit} (Fig. 5a). Due to diffraction phenomena at the interface between an optically thicker and an optically thinner medium, an evanescent electric field is generated at the surface facing the liquid. Fluorophores attached to some component of the cell (TIRF) or

added to the bathing fluid (TIRAF) are excited by the evanescent field. The evanescent field decays exponentially with the distance from the substrate surface. The penetration depth is rather short and is in the order of 100 nm. Fluorophores residing deeper inside the sample than the penetration depth of the evanescent field are not excited. Thus, only fluorophores quite close to the surface contribute to TIRF and TIRAF images.

In TIRF microscopy, transmembrane proteins such as integrins are commonly labeled by a fluorescent tag so that their distribution within the cell–surface junction can be analyzed. For TIRAF microscopy, the extracellular fluid is stained with a water-soluble fluorescent dye instead of staining the cell membrane. When the cells attach and spread, the cellular bodies displace the aqueous phase with the dyes from areas of close cell-to-substrate adhesion [27]. Consequently, cell-covered areas appear dark in TIRAF images, in contrast to TIRF images. Figure 5b shows a typical TIRAF image from the cell–surface junction of an adherent fibroblast. The image shows a non-uniform adhesion along the contact area.

4.1.4 Surface Plasmon Resonance

Surface plasmon resonance (SPR) spectroscopy is another experimental approach to study cell–surface interactions and it is also based on evanescent electric fields. As with the other evanescent wave techniques, the penetration depth of SPR using visible light is below 200 nm. Thus, the sensitivity is confined to the interface between cell and substrate whereas the technique is blind to processes that occur deeper in the sample. It is therefore ideally suited to monitoring cell–substrate interactions, in particular when time-resolved measurements are required [28]. SPR is an emerging technique as far as cell–substrate interactions are concerned but it has a long history as a transducer in biomolecular interaction analysis [29].

As explained before for TIRF and TIRAF, the surface plasmon resonance technique is also based on the phenomenon of total internal reflection and the generation of an evanescent electric field (cf. Figs. 5, 6). In SPR the latter is, however, used to excite surface plasmons (i.e. electron density fluctuations) in a thin layer of a noble metal (most often gold) that is coated on the interface at which total internal reflection occurs. However, surface plasmons are only excited if the resonance condition is precisely met [30]. The resonance condition depends on the angle of incidence, the wavelength of the incident light and the refractive index close to the metal surface. With constant instrument parameters, SPR measures the changes in refractive index of thin layers of inorganic, organic and biological material adsorbed on the thin noble metal surface. As such it has become a very versatile surface-sensitive technique with a myriad of applications.

For a given wavelength of incident light, the excitation of surface plasmons is seen as a dip in intensity of reflected light at a specific angle of incidence (Fig. 6a). This fact opens a whole field of possible optical configurations by which the relationship between reflected light intensity, incident angle and excitation wavelength can be exploited to result in label-free spectroscopic and microscopic

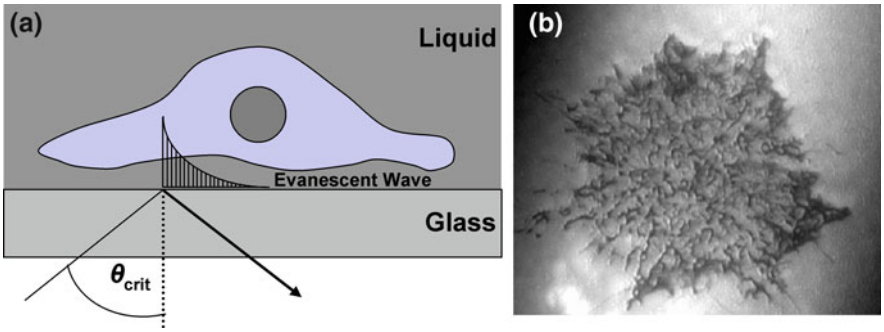

Fig. 5 **a** Schematic illustration of image formation in TIRF/TIRAF microscopy. **b** Typical TIRAF image of the cell–substrate junction (adapted from [27])

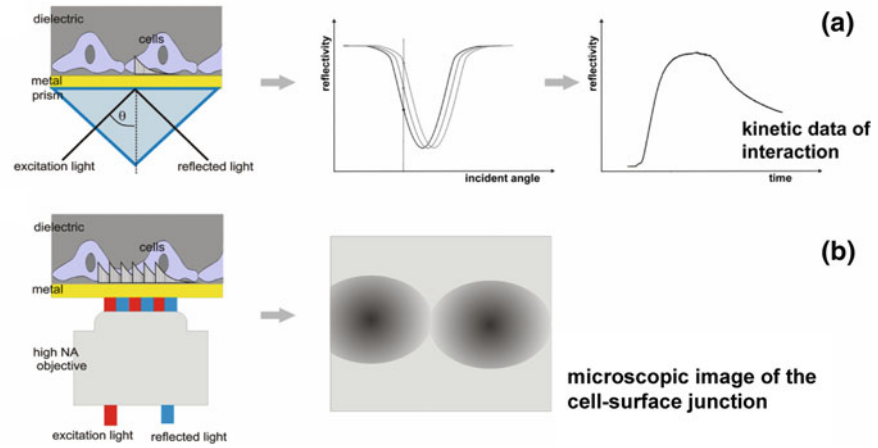

Fig. 6 **a** Kretschmann configuration for performing integral SPR analysis of the cell–surface junction. Surface plasmon excitation is recorded as a dip of the reflectivity as a function of incident angle. During kinetic measurements the changes in reflectivity are acquired at a constant angle of incidence. **b** Setup for SPR imaging based on a high numerical aperture objective

approaches for sensitive and time-resolved analyses of cell–substrate interactions. Most of these approaches are based on the so-called Kretschmann configuration in which the excitation light is coupled into the metal surface via a high refractive index prism for spectroscopic (Fig. 6a) or a high numeric aperture objective for microscopic applications (Fig. 6b). Spectroscopic analyses are performed by either measuring the changes in reflectivity at a constant (monochromatic) excitation wavelength but variable angle of incidence (angle-dependent mode) or by measuring the reflectivity at a constant angle of incidence but with polychromatic excitation and subsequent spectral analysis of the reflected light (wavelength-dependent mode) [29]. In order to perform SPR-based microscopy, a collimated monochromatic light path is used to excite the whole field of view and the reflected

light is recorded by a CCD chip [31]. In this configuration, local changes in refractive index close to the sensor surface are visualized as a microscopic picture (Fig. 6b).

Taken together, there are two ways of studying cell–substrate interactions by SPR: (1) Changes in the refractive index averaged over the entire illumination spot are recorded as a single parameter that integrates over all processes that occur within the evanescent field. (2) SPR-generated reflectivity differences are sampled with lateral resolution and converted into microscopic pictures. Initial SPR studies addressing cell–substrate interactions were conducted in the spectroscopic mode (1) by Yanase et al. in 2007 [32], reporting on their pioneering experiments to grow adherent cells and immobilize suspended cells on SPR sensors. In a subsequent report the group correlated the cell-induced changes in SPR signals and light microscopic images, providing the first correlation between SPR signal strength and the area of cell–surface adherence. The refractive index as an integral parameter that changes when cells—or parts of cells—enter or leave the evanescent field or simply change their morphology was extensively discussed [33]. Cuerrier and Chabot applied SPR successfully to a label-free, time-resolved analysis of changes in cell–cell and cell–surface interactions of human embryonic kidney (HEK) cells when these were stimulated with toxins or physiological agonists or antagonists of cell-surface receptors [34, 35]. Phase-contrast microscopy was used to support a direct correlation of the SPR signal and the cellular reaction which led to changes in cell–surface interactions. The studies clearly showed that SPR detects changes in cell–cell and cell–surface interactions with significantly more sensitivity than phase-contrast micrographs. All of these studies emphasize the pros and cons of the limited penetration depth of the evanescent field. On the one hand the limited decay length of the evanescent field shields off contributions to the signal that do not originate from the cell–surface junction but at the same time it provides a sensitivity problem for cells that do not adhere tightly to their growth surface. This problem has been overcome by the novel concept of FTIR–SPR, which was introduced by Golosovsky et al. [36]. Exciting the surface plasmons with infrared light results in a substantially higher penetration depth of up to 2.5 μm, as the penetration depth corresponds approximately to half the wavelength of the incident light. This setup is capable of conducting a more flexible but still sensitive real-time monitoring of the different phases of the formation of cell–substrate interactions during cell adhesion. Due to the novel quality of the SPR data recorded via infrared excitation, temporal fine structures during adhesion were observed that have not been revealed by other analytical techniques so far [37].

Only a few important studies of surface plasmon resonance microscopy (SPRM) have been published to date. Giebel et al. [31] used SPRM to study cell–substrate interactions of primary goldfish glial cells. Besides the qualitative information obtained from the recorded SPR micrographs about leading and tailing lamellipodia during cell migration, the average distance between surface and different parts of the cell bodies was extracted from the raw data. Comparing SPR data to that from other state-of-the-art microscopic techniques identified the SPRM

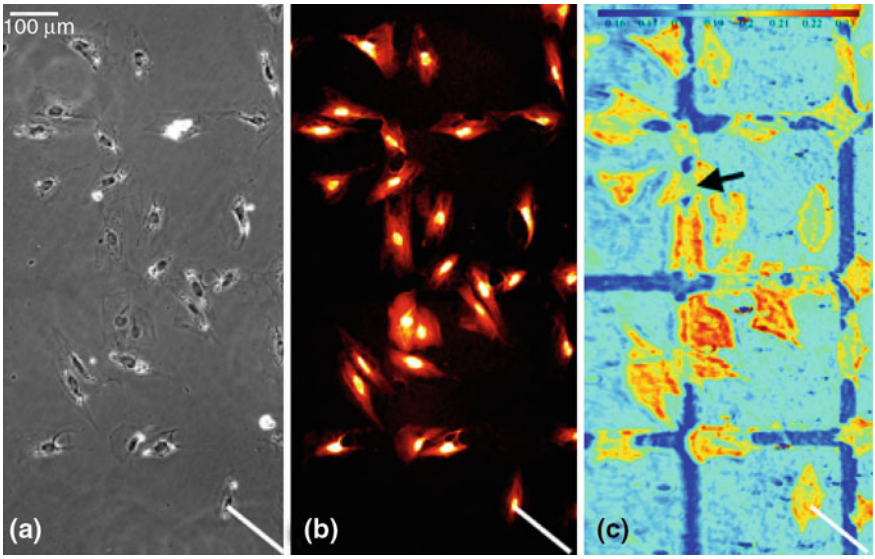

Fig. 7 Vascular smooth muscle cells grown on a substrate with 300 µm squares of fibronectin. The cells had been fixed prior to imaging. **a** Phase-contrast micrograph. **b** Fluorescence micrograph after Texas Red staining. **c** SPR-based micrograph (Adapted from [38])

as a suitable and in some respects even more powerful method for the visualization and quantification of cell–substrate interactions.

Only recently the group of Peterson et al. [38, 39] described an SPRM-based analysis of remodeling processes of the ECM performed by vascular smooth muscle cells during adherence, spreading and migration. By using a sophisticated optical setup and a growth surface carrying fibronectin patterns, the group could simultaneously collect data about the cell density and distance from the matrix as well as the amount of protein that was deposited or removed from the ECM, respectively. Figure 7c compares the SPRM image with conventional phase-contrast microscopy (Fig. 7a) and fluorescence microscopy (Fig. 7b) of the same field of view.

While the sensitivity of the system is remarkably high ($\sim$20 ng/cm^2), the lateral resolution of the micrographs is still low ($\sim$2 µm) compared to other microscopic techniques. Even though SPRM has not been used extensively to study cell–surface adhesion, its unique technical features and readouts may drive further applications.

4.2 Mechanical Methods for Studying the Stability of Cell–Surface Interactions

The mechanical stability of cell–surface interactions can be determined from so-called *detachment assays*. In these assays, substrate-anchored cells are exposed to mechanical forces that aim to detach the cells from the surface under study. The

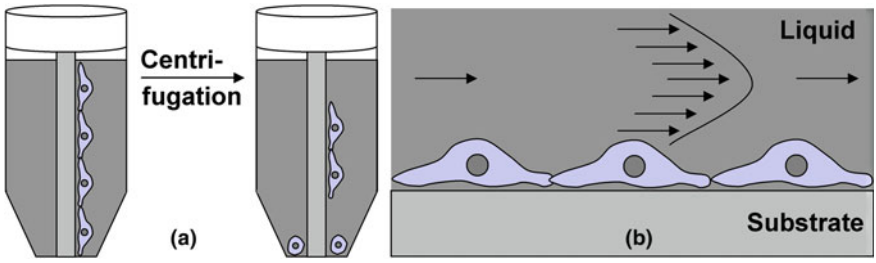

Fig. 8 Detachment assays used to determine the mechanical resistivity in cell–substrate interactions. **a** Centrifugation assay. **b** Hydrodynamic flow assay

more mechanical stress the cells can take without detachment, the more stable are the cell–substrate interactions with the growth surface. Depending on the assay, the mechanical stress is more or less defined and can be gradually increased to find the critical shear force for detachment.

The simplest approach to study cell adhesion strength requires seeding of suspended cells upon a substrate of interest. After a pre-defined incubation time, the surface is rinsed with a physiological washing buffer. Weakly attached cells adhering with a force smaller than the shear forces generated by the flow of buffer are washed from the substrate surface. The number of cells that remain attached to the surface is counted and serves as a measure for the adhesive interactions between surface and cells under study. Although these wash-off assays provide semi-quantitative information about the mechanical stability of cell–substrate interactions, the applied shear forces are ill-defined, difficult to control and of limited use [40].

Thus, more precise assays have been developed that use well-defined shear forces to probe the stability of cell–surface interactions in mature cell populations. According to the type of force application, these assays are classified as centrifugation assays [41, 42] and hydrodynamic shear force assays [43, 44].

4.2.1 Centrifugation Assay

The centrifugation assay (Fig. 8a) applies the shear forces necessary to probe the stability of cell adhesion by centrifugation—as the name implies. After cells are allowed to fully attach and spread upon a surface under study, the cell-covered surfaces are placed into centrifuge tubes filled with culture medium and are centrifuged at a preset angular velocity. The centrifugal force acts as a well-defined shear force parallel to the surface, generating tangential mechanical pull on the cell bodies. After centrifugation the cells which resisted the mechanical stress and remained attached to the substrate surface are counted using microscopic techniques. Repeated runs with increasing angular velocity provide the critical shear force that characterizes the mechanical stability of cell–substrate interactions

for this particular pair of cells and substrate. A quantitative indicator that has been used to describe the strength of cell–substrate interactions is the centrifugal force necessary to detach 50% of the initial cell population. The centrifugation assay is, however, a low-throughput assay as only a single force can be applied per experiment. Moreover, in some cases the strength of cellular adhesion may exceed the forces that can be applied in these assays with reasonable effort.

Channavajjala et al. [41] applied the centrifugation assay to quantify the adhesion strength of tumor cells to immobilized HIV-1 Tat-protein, containing the amino acid sequence RGD, in comparison to other specific ECM proteins such as fibronectin and vitronectin. HIV-1 Tat was shown to mediate cell adhesion, but, unlike the ECM proteins, the interaction between cells and the surface-immobilized protein was mechanically weak.

4.2.2 Hydrodynamic Flow Experiment

In hydrodynamic flow experiments the cell-covered surface is placed in a laminar flow channel and the cells are challenged with increasing flow velocities of the fluid. As in the centrifugation assay, the flow of liquid generates mechanical forces on the cell body tangential to the surface, which may lead to detachment (Fig. 8b). Most frequently a parallel-plate flow apparatus is used. Here the opposing side of the channel is a parallel plate that moves with a preset velocity. A laminar shear flow is generated over the cell surface by viscous coupling of the liquid. In order to guarantee laminar flow the gap height between the parallel plates has to be small compared to the length of the flow path. In a parallel-plate flow chamber the shear stress is constant and depends on the flow rate and the gap between the two plates. Thus, the applied shear stress can be easily adjusted by altering one of these two parameters. After exposing the cells to laminar flow for a definite period of time, the number of adherent cells is counted and compared to the number before the onset of flow, providing the fraction of adherent cells that were capable of resisting a given laminar shear stress.

Using a laminar flow assay Xiao and Truskey [44] analyzed the adhesion strength of endothelial cells grown on a glass substrate that had been pre-coated with linear or cyclic RGD peptides as well as fibronectin. The critical shear stress, defined as the shear stress required to detach 50% of the cells from the coated substrate surface, was determined to be (59 $\pm$ 13) dyne/cm^2 for cyclic and (39 $\pm$ 4) dyne/cm^2 for linear RGD peptide. The value for fibronectin-coated surfaces was lower than those for the peptide coatings.

By mounting the flow chamber on the stage of an inverted phase-contrast microscope and using time-lapse video microscopy, the dynamics of cell detachment can be monitored simultaneously. However, a major limitation of these flow systems is that the detachment forces are usually non-uniform along the cell surface and cannot be calculated without simplifying assumptions about cell shape.

4.3 Electrochemical Approaches for Studying Cell–Surface Interactions

Experimental approaches based on electrochemical impedance analysis—also referred to as impedimetric approaches—are emerging and very versatile research tools for studying cell–substrate interactions in real time. The basic principle of this technique was introduced by Giaever and Keese in 1984 and has been continuously optimized ever since. In the initial publication the technique was named *electric cell–substrate impedance sensing* or short *ECIS* and it has paved the way for several modifications that are all based on the ECIS principles [45]. In ECIS, adherent cells are grown on the surface of planar gold film electrodes, which are pre-deposited on the bottom of a cell culture dish by thin-film technology. The gold films serve as growth substrate for the cells and, at the same time, as electrodes for the electrochemical measurement. With the cells adhering essentially to the electrode surface, there is only a gap of 20–200 nm between the cell bodies and the measurement probe. By virtue of this arrangement the measurement is particularly sensitive to changes that occur within the cell–surface junction in unprecedented detail.

In the most commonly used configuration the measurement system contains two electrodes: a small working electrode (5×10^{-4}cm^2) and a substantially larger ($\sim$500-fold) counter electrode (Fig. 9). The electric circuit is completed by the cell culture medium on top of the cell layer. ECIS is based on measuring changes in the electrochemical impedance of the gold film electrodes at different AC frequencies (alternating current). As the cells behave essentially like insulating particles, they force the current to flow through the cells or around the cell bodies. Both situations result in an increase of the measured impedance due to the presence of the cell bodies on the electrode surface compared to a cell-free electrode.

When initially suspended cells are seeded on an ECIS electrode, it is possible to follow attachment and spreading of the cells upon the electrode surface from time-resolved impedance readings due to the gradual constriction of current flow. ECIS recordings are therefore particularly well-suited to follow the kinetics of cell spreading. Once the cells form a confluent monolayer the impedance becomes stationary as long as the cells do not change their shape. In this situation ECIS is capable of monitoring all experimental challenges that are mirrored by a change in cell shape. As many chemical, physical or biological stimuli result in minute changes of cell morphology, the technique is widely applicable in many research areas that will not be addressed here, such as cytotoxicity screening, GPCR-mediated signal transduction or stem cell differentiation. ECIS readings rely only on small amplitude currents and voltages such that the cells are not affected in any way by the electric field used for the measurement. It is considered to be a non-invasive approach even if the experiment spans several days or even weeks.

The method was originally developed using gold as the electrode material, and gold is by far the most widely used material due to its inertness, its biocompatibility,

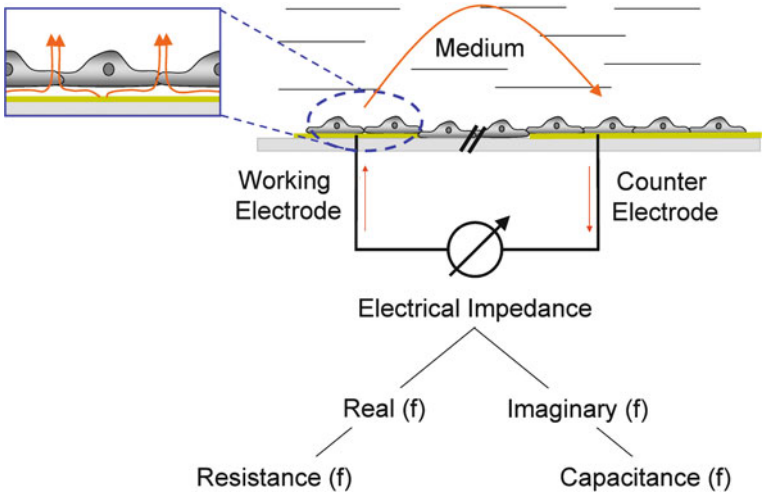

Fig. 9 Schematic of the ECIS principle, indicating AC current flow between the small working electrode and the larger counter electrode via the culture medium. The arrows, which indicate AC current flow, are drawn unidirectional only for the sake of clarity. The size of the electrodes is not drawn to scale with respect to cell size

its electrochemical properties and the well-established concepts for surface modifications. However, the method has been successfully transferred to other electrode materials such as platinum or indium tin oxide (ITO). The latter cases will not be covered in the following paragraphs, which will deal only with ECIS using gold film electrodes. The gold electrodes can be coated with individual components of the ECM or reconstituted preparations of native matrices without losing any sensitivity. Due to their inertness they can be modified by simple adsorption with almost any compound that has to be tested for its impact on cell–substrate adhesion. Moreover, there is an enormous tool box available for modifying the gold surfaces covalently by self-assembly reactions with compounds that carry thiol moieties as functional groups. ECIS is, however, of no use for polymeric or ceramic coatings as these are non conducting and they cannot be coated on the electrodes without losing the ability to perform ECIS readings.

Moreover, ECIS is very well suited to study cell–surface interactions on topographically structured substrates with specific topographical features. For this, inert substrates that carry the topography of interest have to be coated with a thin gold film in a well-defined electrode layout such that impedance readings can be performed with sufficient sensitivity. Characterizing the kinetics of cell attachment and spreading upon topographically structured in vitro surfaces might be of interest before these materials can be used as biomaterials in biosensors or implants.

4.3.1 Monitoring Cell Spreading Kinetics with High Time Resolution

The AC frequency used for ECIS recordings is an extremely important parameter as it determines the current pathway across the cell layer and, thus, the processes that are mirrored in the time-resolved signal. For the electrode size discussed here, the presence of the cells on the electrode surface alters the impedance of the electrode in the frequency range between 10 Hz and 100 kHz. Within this frequency range the current can flow along two different current pathways: (1) *around* the cell bodies via the cell–surface junctions and the cell–cell junctions into the bulk (*paracellular pathway*) or (2) *across* the plasma membranes and directly through the cell bodies (*transcellular pathway*). The first case describes approximately the flow of AC current for frequencies $f < 10$ kHz whereas the latter case describes the current pathway for frequencies $f > 10$ kHz. Thus, selecting the frequency determines where the current flows and as a consequence which part of the cell or which cellular processes are actually probed. A rule of thumb says that whenever morphological changes of the cells are the focus of interest, the measurement should be made sensitive for changes in the paracellular current pathway ($f < 10$ kHz). When coverage of the electrode is of interest—as in spreading and migration experiments—the measurement should be performed in the transcellular frequency regime ($f > 10$ kHz).

According to this rule of thumb, cell attachment and spreading is usually recorded in the high-frequency regime (>10 kHz). At these frequencies, the main part of the current passes capacitively through the cells, passing the basal and the apical cell membrane. For a more detailed analysis of cell spreading kinetics, not the impedance but the capacitive part of the complex impedance (cf. Fig. 9) is followed at a sampling frequency of 40 kHz. When the dielectric cell bodies attach and spread on the electrode surface, they decrease the equivalent capacitance of the electrode at 40 kHz *proportionally* to the fraction of the area they cover [46]. Measuring the capacitance of the system at 40 kHz as a function of time is therefore the most direct approach to monitor the coverage of the electrode surface with time, thus providing the spreading kinetics.

The following examples illustrate the analytical performance of the device. Figure10a shows the kinetics of cell spreading for epithelial MDCK (Madin–Darby canine kidney) cells seeded on ECIS electrodes that were pre-coated with different ECM proteins [46]. The time courses of the individual electrode capacitances at a sampling frequency of 40 kHz show clear differences in the time to confluence on these different ECM proteins. The electrode capacitance decreases as the cells spread out on the electrode surface. Whereas cell attachment and spreading is fastest on a fibronectin-coated electrode, spreading on the non-adhesive serum albumin (BSA) takes significantly longer. Thus, the individual spreading kinetics provide quantitative information on the interaction of the cells under study with this particular protein coating.

Two parameters can be extracted to describe the adhesion and spreading kinetics on the different proteins quantitatively: the parameter $t_{1/2}$ provides the time required for half-maximal cell spreading and the parameter s stands for the

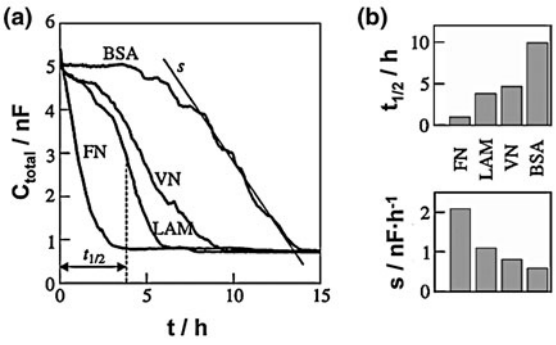

Fig. 10 Monitoring attachment and spreading of suspended cells by ECIS recordings. **a** Time course of the electrode capacitance at 40 kHz during attachment and spreading of initially suspended MDCK cells seeded at time point zero on ECIS electrodes pre-coated with different ECM proteins (FN = fibronectin, VN = vitronectin, LAM = laminin, BSA = bovine serum albumin). **b** Half-times $t_{1/2}$ and spreading rates *s* as determined from the data in a

spreading rate. The spreading rate is deduced from the slope of the curve at $t=t_{1/2}$ (Fig. 10a). It is directly proportional to the adhesion energy of the cells with a given surface composition [47]. $t_{1/2}$ values for the different protein coatings clearly mirror the time courses of the electrode capacitance, identifying BSA as the least adhesive protein with the highest $t_{1/2}$ value. However, the spreading rate *s* for BSA is close to the values for LAM and VN, indicating a similar adhesion energy for BSA compared to these two proteins (Fig. 10b).

This apparent discrepancy is readily explained by the onset of ECM production in the cells that were seeded on BSA-coated electrodes. The absence of adhesion sites on the surface triggers ECM production and secretion.

4.3.2 Monitoring Micromotion within Confluent Monolayers

Besides the kinetics of cell attachment and spreading, ECIS is also capable of recording metabolically driven cell shape fluctuations that have been referred to as micromotion [48]. Micromotion recordings integrate over transient and minute changes in cell–cell contacts, cell–substrate contacts, cell volume and cell membrane invaginations. The scale of these cell shape fluctuations can be in the sub-nanometer range and still be visible in ECIS measurements. Micromotion has been electrically recorded as small and rapid fluctuations of the impedance of cell-covered ECIS electrodes, when the impedance is tracked as a function of time at a single frequency sensitive for these movements. According to the rule of thumb described in the preceding paragraph, micromotion recordings are typically performed at intermediate frequencies, most often at 4 kHz. The higher the time resolution of the measurement the more of the inherent dynamics of the cell layer is revealed. Thus, micromotion recordings provide direct and indirect information

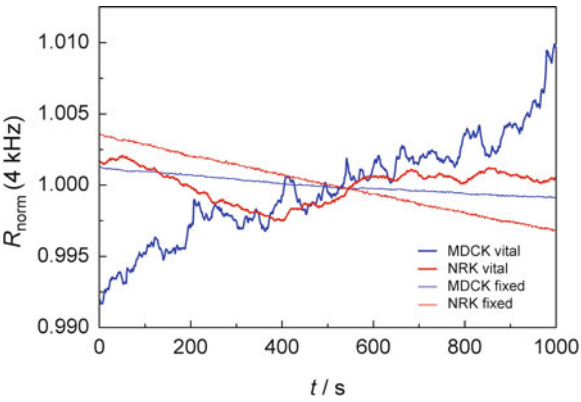

Fig. 11 Cellular micromotion as revealed in time-resolved measurements of the normalized resistance of an ECIS electrode covered with a confluent monolayer of MDCK (*blue*) or NRK cells (*red*) before (*thick lines*) and after fixation (*thin lines*) with formaldehyde. The resistance was measured at 4 kHz each time

about the cytocompatibility of a given surface—via direct contributions from the cell–surface junction to the observed impedance fluctuations, and indirectly since micromotion is a general indicator of cell viability [49].

Figure 11 compares the micromotion of two different cell lines before (thick lines) and after (thin lines) the cells were fixed with formaldehyde. Different cell lines show individual and characteristic "fingerprints" of their motility whereas dead cells no longer induce any significant resistance fluctuations anymore. Analysis of micromotion for different electrode coatings may provide valuable insights into the interactions between cells and a given surface.

4.3.3 Monitoring Cell Migration

Cell–surface interactions play an important role in the ability of a cell to migrate, as, for instance, during wound healing or embryonic development. The easiest assay for assessing cell migration on a given ECM in vitro is called the *wound healing scratch assay*: a confluent cell monolayer grown on the surface under study is mechanically wounded by scratching the tip of a pipette or a needle through the cell layer. The size of the lesions depends on the size of the needle. Cells from the periphery of the scratch migrate into the center of the wound and this process can be documented and analyzed microscopically over time. A weakness of this assay is the time-consuming analysis of the micrographs and the fact that the applied mechanical wounds are often hard to reproduce. The assay becomes significantly more reproducible and more convenient when the cell layer is established on ECIS electrodes such that the electrodes can be used to apply a lethal electric field and thereby wound those cells residing on the electrode surface. When the conditions of the electric wounding pulse are properly selected, all the cells on the electrode surface die but not those in the periphery of the electrode (Fig. 12). Migration of viable cells from the electrode periphery to the center of the electrode (*wound healing*) can be followed quantitatively by time-resolved ECIS

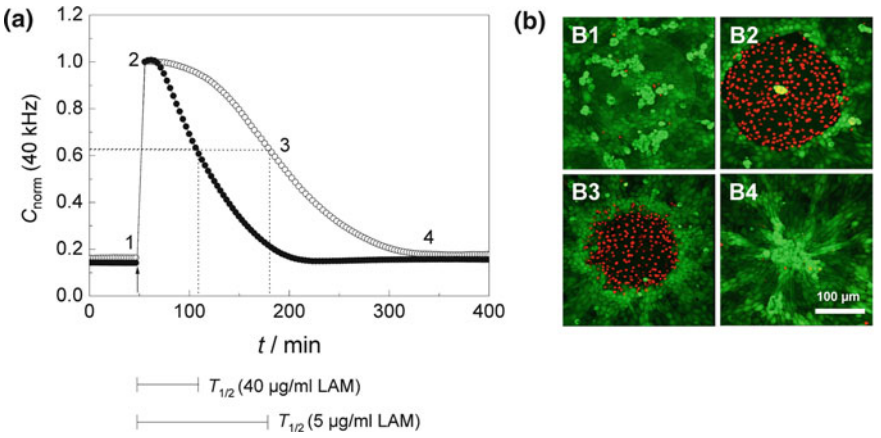

Fig. 12 ECIS-based cell migration assay. **a** Time course of the normalized capacitance measured at an AC frequency of 40 kHz along a complete wound healing/migration assay with NRK cells grown on ECIS electrodes pre-coated with 40 µg/mL (*filled circle*) or 5 µg/mL (*open circle*) laminin. Numbers 1–4 indicate the time points at which a vital stain of the cells on the electrode was performed (cf. Fig. 12b). $T_{1/2}$ is the time to reach half-maximal repopulation of the electrode. Capacitance data was normalized to the first value after electrical wounding (cell-free electrode). **b** Fluorescence micrographs of NRK cells stained with calcein AM and ethidium homodimer-1 at different points of the wound healing/migration assay (green = vital cells, red = dead cells; the staining was performed **1:** before, **2:** immediately after the wounding pulse, **3:** after 50% wound healing, and **4:** after complete wound healing)

readings [50]. In contrast to the mechanical scratch assay, the ECIS-based wound healing assay provides well defined and highly reproducible wounds, as they correspond to the size of the electrode.

Similar to cell attachment and spreading studies, the capacitance at a sampling frequency of 40 kHz is the most useful indicator for monitoring the repopulation of the electrode surface by cells migrating in from the periphery. Figure 12a shows the time course of the normalized capacitance at 40 kHz after wounding a confluent layer of NRK cells that have been grown on ECIS electrodes pre-coated with laminin (LAM) in different concentrations. The arrow at position 1 marks the time point when the invasive electric field was applied to the cells, killing the cells on the electrode. Immediately after pulse application the capacitance increases from its minimum value, which mirrors a confluent cell layer, to a typical reading for an open, cell-free electrode. The electrical permeabilization of the cell membranes allows the current to flow freely through the dead cells without a measurable capacitance contribution from the cell membranes. As time progresses C_{norm} continuously decreases back to the pre-pulse values as the electrode is gradually repopulated by cells that migrate in from the periphery. The rate of the capacitance decrease depends on the LAM concentration. Eventually, the capacitance reaches the stationary level of a cell-covered electrode again, indicating that the healing process is completed (closure of the wound). To characterize the assay readout for different electrode coatings by a single parameter, it is useful to

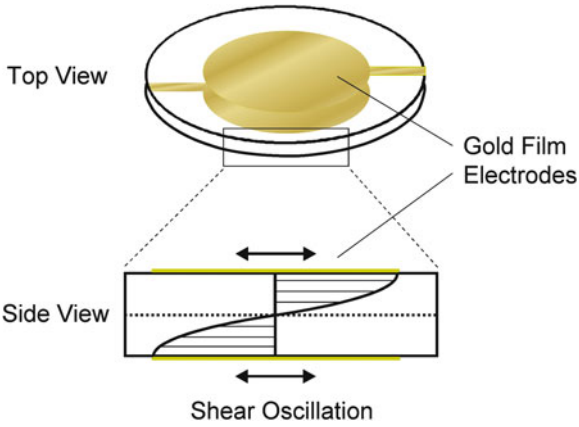

Fig. 13 *Top* and *side* views of a shear wave resonator as used in QCM-based experiments. The quartz resonator is sandwiched between two gold film electrodes used to drive the resonant oscillation and to read the resonance frequency. Under resonance conditions a standing acoustic wave is established between the crystal's surfaces. Resonance parameters are very sensitive to adsorption or desorption processes at the surface

determine the time $T_{1/2}$ needed to attain half-maximal capacitance decrease after wounding and, thus, half-maximal repopulation of the electrode (= wound healing). The slope of the capacitance versus time curves mirrors the migration velocity.

Fluorescence microscopic observation of the ECIS-based wound healing assay (Fig. 12b) provides images of the different stages of the wound healing process. A fluorescence-based viability assay based on ethidium homodimer-1 (EthD-1; red fluorescence) and calcein acetoxymethylester (CaAM; green fluorescence) was used to discriminate live and dead cells in the micrographs at the times indicated in Fig. 12a. The DNA-intercalating dye EthD-1 is a marker for membrane integrity as it is non-membrane-permeable and can only access the nuclei after membrane permeabilization. Calcein AM (CaAM) is essentially non-fluorescent but membrane-permeable. Intracellular esterases inside living cells hydrolyze CaAM to the membrane-impermeable calcein, which emits a green fluorescence. Before the high-field application, all cells exhibit a green cytoplasmic fluorescence, which thus indicates vital cells. After the elevated field is applied, all cells residing on the electrode are selectively wounded as indicated by their EthD-1 stained cell nuclei (red), while the cells surrounding the electrode remain vital, showing a green cytoplasmic fluorescence (Fig. 12b2). Figure 12b3 shows a fluorescence image of an electrode covered with NRK cells after half-maximal wound healing. A radial growth pattern in the cell layer near the electrode periphery can be observed as the cells have migrated inward, suggesting a re-alignment of the cells during the migration process. This pattern is even more pronounced for the image recorded after wound closure (Fig. 12b4).

4.4 Acoustic Techniques for Studying Cell–Surface Interactions

Several acoustic approaches have been described that are capable of providing valuable information about the formation and modulation of cell–surface interactions. By far the most widely known device is the quartz crystal microbalance

(QCM) that has a long track record as a mass-sensitive tool to study adsorption reactions at the solid–liquid interface. It operates non-invasively and with a superb time resolution that is much better than necessary for most cell-related studies. The core component of this technique is a thin, disk-shaped piezoelectric (AT-cut) quartz crystal sandwiched between two gold film electrodes. When an oscillating potential difference is applied between the surface electrodes, the piezoelectric resonator is excited to perform mechanical shear oscillations parallel to the crystal faces at the resonator's resonance frequency (Fig. 13). This mechanical oscillation is highly sensitive to changes that occur at the resonator surface, so that adsorption or desorption processes can be followed by readings of the resonance frequency f [51] or by analyzing the shear oscillation of the resonator using principles of impedance analysis [52–54].

For many years the QCM technique was used as an established and accepted tool for studying deposition processes of thin material films in the gas phase or in vacuum. As long as the adlayer film is rigid and homogeneous, the resonance frequency decreases in proportion to the amount of deposited mass [55], providing a balance with nanogram sensitivity. Recent progress in designing better oscillator circuits to determine the resonance frequency or alternative readout approaches has paved the way to monitor adsorption processes even in an aqueous environment—a prerequisite for the detection of protein adsorption or cell adhesion processes under physiological conditions.

4.4.1 Monitoring Attachment and Spreading on Protein-Coated Resonators

The most sensitive operational mode for a quartz resonator is the *active oscillator mode*. Here, the quartz resonator is integrated as the frequency-controlling element in an oscillator circuit and the resonance frequency of the crystal is recorded with high sensitivity and a time resolution of less than 1 s. The oscillator circuit only compensates for energy losses and maintains the quartz resonator at its resonance frequency. The general applicability of the QCM technique in the active oscillator mode for studying cell adhesion has been demonstrated by various authors addressing a variety of bioanalytical issues. Gryte et al. [56], Redepenning et al. [57] and Wegener et al. [58] monitored the attachment and spreading of initially suspended mammalian cells on the resonator surface in real time by readings of the resonance frequency. They showed that the attachment and spreading of mammalian cells upon the resonator surface induced a decrease in the resonance frequency that was proportional to the fraction of the surface area covered with cells (Fig. 14). Thus, time-resolved measurements of the resonance frequency mirror the kinetics of cell attachment and spreading on the resonator surface. To illustrate the quality of the data, Fig. 14a shows the time course of the resonance frequency shift when increasing amounts of MDCK cells are seeded on the resonator surface at time zero. After a transient slight increase of the resonance frequency due to warm-up of the medium, Δf decreases, reporting on the

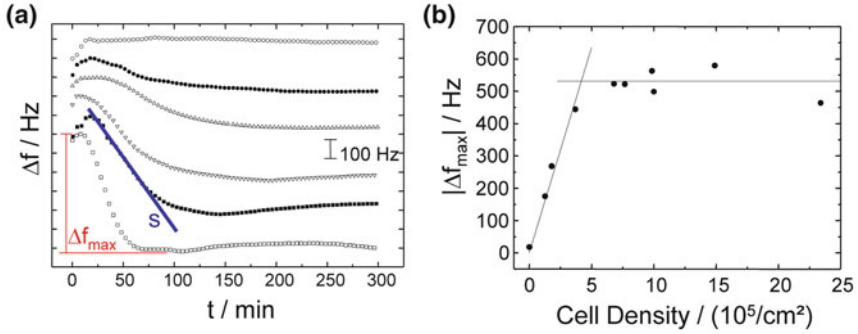

Fig. 14 **a** Shift in resonance frequency during attachment and spreading of initially suspended MDCK cells. From the upper to the lower curve seeding densities (in $10^5 cm^{-2}$) increase (*open circle* 0; *filled circle* 1.3; *triangle* 1.8; *filled down triangle* 3.7; *filled square* 7.7; *open square* 15). Δf_{max} indicates the maximum frequency shift observed for a given seeding density. **b** Maximum frequency shift Δf_{max} as a function of the cell density seeded on the resonator surface at time point zero. T = 37 C

continuous progress in cell attachment and spreading. The total shift in resonance frequency (Δf_{max}) increases with increasing seeding density up to a threshold value. This becomes obvious when the total frequency shift is plotted against the number of seeded cells, providing a saturation curve (Fig. 14b).

For low seeding densities the frequency shift is proportional to the fractional surface coverage with cells. However, when all adhesion sites on the surface are occupied by cells, the frequency shift does not further increase even though the number of seeded cells is further raised. This observation confirms that only those cells in direct contact with the resonator surface contribute to the QCM signal.

Wegener et al. [58], who studied the adhesion of different mammalian cell types, have additionally found that confluent monolayers of different cell types produce individual shifts in resonance frequency, possibly reflecting individual molecular architectures of their cell–substrate contacts. With a more detailed understanding of this cell-type-specific QCM readout, unprecedented information about the interactions of cells with in vitro surfaces will become available. This next step requires methodological improvements with more observables than just the resonance frequency. The resonance frequency of the quartz resonator is an integral parameter sensitive to both mass deposition and changes in the density or viscosity of the material in contact to the resonator surface [59]. Discrimination between these two contributions is not possible from readings of the resonance frequency alone. This, however, becomes important when the resonator is loaded with a complex material that neither behaves like a rigid mass nor has uniform contact with the surface. Cells are viscoelastic bodies for which the linear relationship between adsorbed mass and change in frequency is not valid [60, 61]. Rodahl et al. [61, 62] developed an extension of the traditional QCM technique,

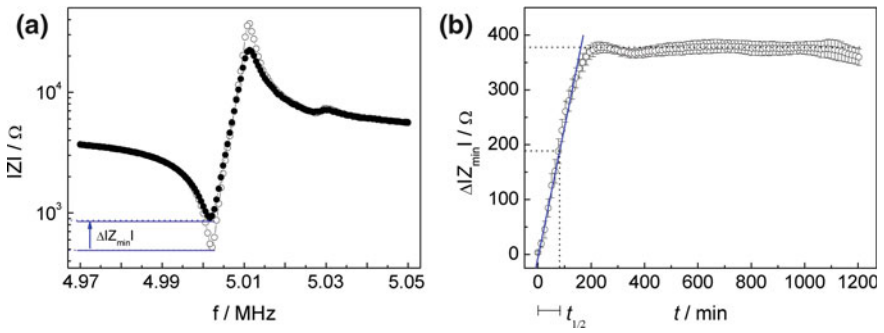

Fig. 15 **a** Impedance spectra near resonance of a cell-free (*open circle*) and a cell-covered (*filled circle*) 5-MHz quartz resonator. The arrow indicates the change of the minimal impedance $\Delta|Z_{min}|$, which was used to follow cell attachment and spreading upon the resonator surface. **b** Time course of the minimal impedance $\Delta|Z_{min}|$ during the attachment and spreading of NRK cells upon the quartz resonator. Changes of the load parameters are given relative to a cell-free but medium-loaded resonator. $t_{1/2}$ is the time required to induce a half-maximal change of $\Delta|Z_{min}|$. Mean ± SEM, n = 5; T = 37 C

the so-called QCM-D technique, which provides measurements of the dissipation factor D in addition to the common measurement of the resonance frequency f. The dissipation factor quantifies the damping of the quartz oscillation and is defined as the ratio of the dissipated energy to the energy that is elastically stored during one period of oscillation. Simultaneous f and D measurements are performed by periodically switching off the driving power to the quartz oscillator and subsequently recording the free decay of the quartz oscillation. The measured decay time of the damped sine wave is expressed as the dissipation factor, to which it is inversely proportional. Readings of D indicate whether the recorded shift in resonance frequency arises from dissipative processes, as occur with any viscous loading of the resonator surface [61]. Thus, simultaneous f and D measurements facilitate the detailed interpretation of QCM experiments.

Fredriksson et al. [63] and Nimeri et al. [64] used this approach to characterize the attachment and spreading of mammalian cells and the interaction of neutrophils with a protein-coated surface. Reiss et al. [65] used functionalized (biotin-doped) lipid vesicles and studied their adhesion onto a resonator surface coated with specific ligands (avidin) as a simple model system to mimic cell attachment and spreading. The adhesion of mammalian cells and liposomes gave rise to very similar shifts in resonance frequency, whereas the viscous energy dissipation was at least one order of magnitude higher when cells made contact with the resonator. As a conclusion of these studies it was obvious that the viscous properties of the cell–surface junction and the cell body had a great impact on QCM readings.

The second operational mode for QCM experiments is termed the *passive mode*. Here, the quartz resonator is not oscillating freely but a sinusoidal voltage is applied to the surface electrodes and the crystal is thereby forced to oscillate at frequencies determined by the frequency of the applied AC voltage. The quartz is

excited sequentially along a narrow frequency band around its fundamental resonance and the electrical impedance of the system is recorded. Figure 15a shows a typical impedance spectrum for a medium-loaded resonator compared to the same resonator covered with a confluent monolayer of NRK cells.

The presence of cells on the resonator surface is most obviously expressed by a significant damping of the shear oscillation as indicated by shifts of the minimal ($|Z_{min}|$) and the maximal impedance ($|Z_{max}|$). Attachment of the cells to the resonator induces only a minor shift of the impedance spectrum along the frequency axis towards lower frequencies. This confirms that the cell monolayer induces primarily dissipation of motional energy and only a negligible storage of elastic energy.

Attachment and spreading of initially suspended cells to the resonator surface is followed over time by continuously recording impedance spectra such as the one shown in Fig. 15a. The gradual coverage of the surface is mirrored in the change of the minimal impedance magnitude $\Delta|Z_{min}|$, which is directly extracted from the raw data (blue horizontal lines in Fig. 15a), as a function of time (Fig. 15b). Figure 15b shows the time course of the minimal impedance $\Delta|Z_{min}|$ during the attachment and spreading of initially suspended NRK cells seeded to confluence upon the resonator surface, expressed relative to the value for the medium-loaded resonator. Immediately after cell inoculation (t = 0), $\Delta|Z_{min}|$ shows a characteristic steep increase, reaching a stationary value once spreading is complete. Since the cells were seeded to confluence into the measuring chamber, i.e. they already cover the entire quartz surface after sedimentation and adhesion without any need for further cell proliferation, the final change in $\Delta|Z_{min}|$ corresponds to a confluent monolayer of cells on the surface. The initial increase of $\Delta|Z_{min}|$ with time describes the kinetics of cell attachment and spreading, which is quantified by two parameters, $t_{1/2}$ and s. The quantity $t_{1/2}$ describes the time that is needed to reach the half-maximal change of $\Delta|Z_{min}|$, which corresponds to half-maximal surface coverage. The slope s of the attachment curve quantifies the spreading rate and is directly proportional to the adhesion energy of the cells.

With the help of these different operational modes it is possible to unravel several key features of any QCM-based analysis of cell–surface junctions:

1. QCM readings only report on specific, integrin-mediated cell adhesion to the resonator surface. Sedimentation and loose attachment of cells to the resonator surface via nonspecific interactions do not influence the QCM readout [58, 66].
2. QCM readings are only sensitive to those parts of the cellular body that are involved in making cell–substrate contacts and that are close to the resonator surface [66]. Thus, sensitivity is confined to the cell–surface junction.
3. The presence of a confluent cell layer on top of the resonator surface leads to a significant increase in viscous energy dissipation, usually many times (2- to 10-fold) larger than the increase in the stored energy [67]. The impact of cells on energy dissipation was shown to be cell-type-dependent reflecting individual acoustic properties.

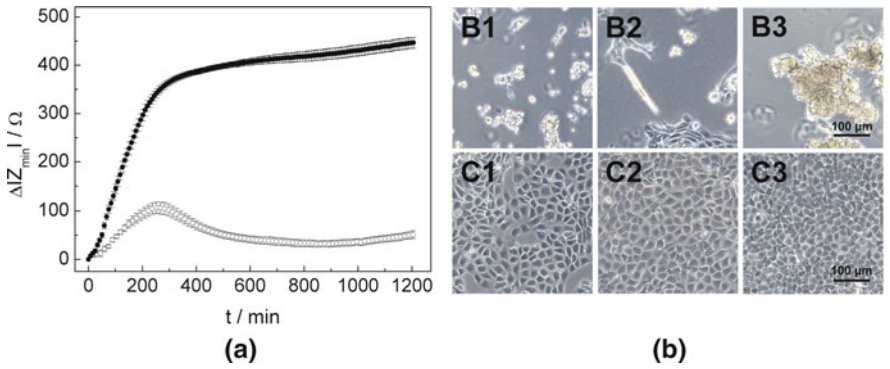

Fig. 16 **a** Time course of $\Delta|Z_{min}|$ after seeding equal numbers of initially suspended NRK cells on a polystyrene-coated quartz resonator at time point zero. The PS film on the resonator was either left unmodified (*open circle*) or had been exposed to an argon plasma (*filled circle*) prior to inoculation. The value of $|Z_{min}|$ at the beginning of the experiment was set to zero. (Mean ± SEM,n ≥ 5;*T* = 37 C). **b** Phase-contrast micrographs of NRK cells 10 h (**1**), 24 h (**2**) and 48 h (**3**) after inoculation on unmodified PS (*B1*, *B2*, *B3*) and plasma-treated PS (*C1*, *C2*, *C3*)

4. A major contributor to the QCM signal of adherent cells is the actin cytoskeleton [66]. Taken together with point (2) above, it is the part of the actin cytoskeleton associated with cell–surface junctions that contributes to the QCM signal and can be probed by QCM experiments.

4.4.2 Biocompatibility Testing of Polymer Surfaces

In contrast to the electrochemical approaches described in the preceding section, which are limited to conductive coatings of the electrodes with proteins or other biomolecules, the QCM-based analysis of cell–surface interactions is also applicable to polymeric, metallic or ceramic coatings of the resonator. Any of these materials can be coated as a thin film on the resonator surface and then resonance analysis is performed just as described above. The only requirements with respect to material deposition are homogeneity and rigidity of the coating such that no significant acoustic loss occurs within the adlayer, as this would reduce the inherent sensitivity of the resonator for subsequent cell adhesion studies. Figure 16a shows the time course of attachment and spreading of NRK cells after a single-cell suspension was seeded to confluence on a quartz resonator coated with a thin layer of polystyrene (PS). Spreading kinetics are again mirrored in the time course of $\Delta|Z_{min}|$. When initially suspended NRK cells are seeded on an unmodified PS surface (open symbols), the minimal impedance $\Delta|Z_{min}|$ shows only a minor and transient increase, indicating that specific interactions between cells and the underlying surface are not allowed to form. Apparently, the cells are not able to attach and spread properly on this surface. By contrast, after a selective hydrophilization of the PS surface by short-term exposure to an argon plasma, cell

attachment and spreading occurs immediately (filled symbols in Fig. 16a). $\Delta|Z_{min}|$ increases to a transient maximum within 350 min after cell inoculation and even continues to increase to a final maximum. These results were confirmed by phase-contrast micrographs recorded 10, 24 and 48 h after seeding of the NRK cell suspension on both polymer surfaces (Fig. 16b).

On the unmodified PS surface only a small fraction of the seeded cells has spread on the surface within 10 h (Fig. 16b1), whereas the predominant fraction remains spherically shaped and forms clump-like aggregates floating in the culture medium. 24 h after cell inoculation, small cell islets have formed (Fig. 16b2) showing individual cells with a quite untypical, elongated morphology. 48 h after cell inoculation, no adherent cells can be observed on the unmodified PS surface but large aggregates of cell fragments and apoptotic cells are floating in the culture medium (Fig. 16b3). By contrast, 10 h after cell inoculation upon the plasma-treated surface, the biggest fraction of the surface is covered with spread cells (Fig. 16c1). As time progresses a confluent cell monolayer is established with a gradual increase in the cell number per unit area (Fig. 16c2, c3).

Compared to microscopic studies, an inherent advantage of the QCM approach is that it directly provides quantitative and time-resolved data of cell spreading kinetics without any need for complex and time-consuming image analysis. The inability of cells to attach and spread upon unmodified, hydrophobic PS is in good agreement with the literature [68–70] and might be related to the pre-adsorbed protein layer which influences the behavior of cells approaching the surface. On hydrophobic surfaces like unmodified PS, the soluble proteins are thought to adsorb under conformational rearrangement (denatured conformation) on the polymer surface, making the binding sites within the adsorbed proteins inaccessible to cell–surface receptors. Consequently, specific cell–substrate contacts cannot be established and cell adhesion is almost completely inhibited. On the other hand, PS surfaces after argon plasma treatment generally allow the proteins to adsorb without unfolding, rendering the surface cytocompatible. Consequently, the integrin binding sites within the adsorbed proteins should be accessible for the cell-surface receptors of the arriving cells. This single example shows the general applicability of the QCM approach to study the biocompatibility of different biomaterials, no matter whether they are polymers, metals or ceramics.

4.4.3 Probing the Cell–Surface Junction Under Shear Stress

In the preceding paragraphs the QCM-device has been described as a *sensor* to monitor the mechanical interactions between cells and surface. It can also be used as an *actuator* capable of disturbing or even dissolving molecular recognition at the solid–liquid interface, such as cell–surface contacts. In the *actuator mode*, the resonator is used at an elevated lateral shear amplitude. The latter is controlled by the driving voltage applied to the surface electrodes to excite the crystal. Heitmann and Wegener [71] studied the impact of elevated lateral oscillation amplitudes on the adhesion kinetics of different mammalian cells. By gradually increasing the

Table 1 Analytical techniques capable of probing cell–surface interactions

Technique	Information provided	Substrate	Strength	Limitation
RICM Microscopic/ Optical	Images of contact area between living cells and growth substrate	transparent glass substrate	• non-invasive • high time resolution • readout confined to cell–surface junction	• areas with very thin cells or cell protrusions cannot be analyzed • cell–substrate separation distance cannot be quantified reliably
FLIC Microscopic/ Optical	Distance between lower cell membrane and surface with high precision	silicon substrate with steps of silicon dioxide	• most precise determination of cell–substrate separation distance	• requires membrane staining by lipophilic membrane dye; • requires Si-substrate with steps of SiO_2
TIRF/TIRAF Microscopic/ Optical	*TIRF*: identification of molecular components close to the growth surface after specific labeling	transparent glass substrate	• readout confined to cell–surface junction	•*TIRF*: requires fluorescent membrane staining
	TIRAF: images of contact area between living cells and growth substrate		• detailed image of cell–surface junction	•*TIRAF*: requires fluorescent staining of extracellular buffer
SPR Optical	Refractive index of material within hundreds of nm from the surface; used as integral readout parameter for cell coverage	gold film of precise thickness on glass substrate with specified refractive index	• label-free and non-invasive • high time resolution • readout confined to cell–surface junction	• interpretation of integral refractive index still difficult • limited parallelization
Flow-Induced Mechanical	Quantitative assessment of the shear resistance of cell–surface interactions	all substrates	• applicable to all substrates • direct mechanical information	• invasive • no time-resolved information • requires cell counting

(continued)

Table 1 (continued)

Technique	Information provided	Substrate	Strength	Limitation
ECIS Electrochemical	Cell spreading kinetics, micromotility of adherent cells, migration velocity in wound healing assay	planar gold film electrodes	• label-free and non-invasive • 96 samples in parallel • automated assay • real time approach	• restricted to conducting and electrochemically well-behaved electrode materials • sensitive to cell morphology as competing signal contribution
QCM Acoustic	Cell spreading kinetics, micromechanics of cell–surface junction, shear resistance of cell–surface interactions	piezoelectric quartz crystal sandwiched between two gold film electrodes	• label-free and non-invasive • real time approach • resonator can be coated with any thin and rigid material	• limited parallelization • sensitive to cellular micromechanics as competing signal contribution

amplitude of the resonator's shear displacement during cell attachment, the authors were able to determine a threshold lateral oscillation amplitude of ~20 nm in the center of the resonator (driving voltage: > 5 V) beyond which cell adhesion to the quartz surface was retarded or even entirely blocked. A maximum shear amplitude of 35 nm (driving voltage: 10 V) was sufficient to completely inhibit cell adhesion for all cell lines under study. However, shear oscillations of similar amplitudes were unable to disrupt cell–surface interactions within established cell layers. The cells could not be displaced from the surface once they had formed mature adhesions. In the long run, this method might develop into a new approach to probe the mechanical shear resistance of cell–surface interactions. As it is possible to coat the resonator with different biomaterials without losing its sensor function, the assay can be used to characterize a wide variety of materials.

5 Synopsis

Table 1 summarizes the various approaches and techniques for studying cell–surface interactions as they have been described in this survey. We have included the individual strengths and limitations of each technique according to our personal perspective and judgment. The survey is not exhaustive but focuses on those assays and concepts that have given or are expected to give significant input to a better understanding of cell–surface interactions.

Acknowledgments The authors would like to express their gratitude to the Kurt-Eberhard Bode Stiftung (Germany) for financial funding.

References

1. Davies JA (2001) Encyclopedia of Life Sciences. Wiley, Chichester www.els.net
2. Ziats NP, Miller KM, Anderson JM (1988) Biomaterials 9:5
3. Lee JH, Khang G, Lee JW, Lee HB (1998) J Colloid Interface Sci 205:323
4. Vogler EA (1998) Adv Colloid Interface Sci 74:69
5. Norde W, Haynes CA (1995) In: Horbett TA, Brash JL (eds) Proteins at interfaces II: fundamentals and applications, American Chemical Society, Washington, p 26
6. Roach P, Farrar D, Perry CC (2005) J Am Chem Soc 127:8168
7. Bongrand P (1998) J Dispersion Sci Technol 19:963
8. Pierres A, Benoliel AM, Bongrand P (2002) Eur Cell Mater 3:31
9. Arnaout MA, Mahalingam B, Xiong J-P (2005) Annu Rev Cell Dev Biol 21:381
10. Hynes RO (1992) Cell 69:11
11. Barczyk M, Carracedo S, Gullberg D (2010) Cell Tissue Res 339:269
12. Wegener J (2006) Wiley encyclopedia of biomedical engineering, vol 6. Wiley, Hoboken, p 1
13. Krissansen GW, Danen EH (2006) Encyclopedia of life sciences. Wiley, Chichester www.els.net
14. Krissansen GW, Danen EH (2007) Encyclopedia of life sciences. Wiley, Chichester www.els.net

15. Wozniak MA, Modzelewska K, Kwong L, Keely PJ (2004) Biochim Biophys Acta 1692:103
16. Pierschbacher MD, Ruoslahti E (1984) Nature 309:30
17. Bokel C, Brown NH (2002) Dev Cell 3:311
18. Cox EA, Huttenlocher A (1998) Microsc Res Tech 43:412
19. Hynes RO (2002) Cell 110:673
20. Luo BH, Carman CV, Springer TA (2007) Annu Rev Immunol 25:619
21. Verschueren H (1985) J Cell Sci 75:279
22. Curtis ASG (1964) J Cell Biol 20:199
23. Schindl M, Wallraff E, Deubzer B, Witke W, Gerisch G, Sackmann E (1995) Biophys J 68:1177
24. Braun D, Fromherz P (1997) Appl Phys A-Mater Sci Process 65:341
25. Lambacher A, Fromherz P (1996) Appl Phys A-Mater Sci Process 63:207
26. Truskey GA, Burmeister JS, Grapa E, Reichert WM (1992) J Cell Sci 103(Pt 2):491
27. Geggier P, Fuhr G (1999) Appl Phys A-Mater Sci Process 68:505
28. Su YD, Chiu KC, Chang NS, Wu HL, Chen SJ (2010) Opt Express 18:20125
29. Robelek R (2009) Bioanal Rev 1:57
30. Knoll W (1998) Annu Rev Phys Chem 49:569
31. Giebel KF, Bechinger C, Herminghaus S, Riedel M, Leiderer P, Weiland U, Bastmeyer M (1999) Biophys J 76:509
32. Yanase Y, Suzuki H, Tsutsui T, Uechi I, Hiragun T, Mihara S, Hide M (2007) Biosens Bioelectron 23:562
33. Yanase Y, Suzuki H, Tsutsui T, Hiragun T, Kameyoshi Y, Hide M (2007) Biosens Bioelectron 22:1081
34. Chabot V, Cuerrier CM, Escher E, Aimez V, Grandbois M, Charette PG (2009) Biosens Bioelectron 24:1667
35. Cuerrier CM, Chabot V, Vigneux S, Aimez V, Escher E, Gobeil F, Charette PG, Grandbois M (2008) Cell Mol Bioeng 1:229
36. Golosovsky M, Lirtsman V, Yashunsky V, Davidov D, Aroeti B (2009) J Appl Phys 105
37. Yashunsky V, Lirtsman V, Golosovsky M, Davidov D, Aroeti B (2010) Biophys J 99:4028
38. Peterson AW, Halter M, Tona A, Bhadriraju K, Plant AL (2009) BMC Cell Biol 10
39. Peterson AW, Halter M, Tona A, Bhadriraju K, Plant AL (2010) Cytometry Part A 77A:895
40. Sagvolden G, Giaever I, Pettersen EO, Feder J (1999) Proc Natl Acad Sci USA 96:471
41. Channavajjala LS, Eidsath A, Saxinger WC (1997) J Cell Sci 110(Pt 2):249
42. Thoumine O, Ott A, Louvard D (1996) Cell Motil Cytoskeleton 33:276
43. Truskey GA, Pirone JS (1990) J Biomed Mater Res 24:1333
44. Xiao Y, Truskey GA (1996) Biophys J 71:2869
45. Giaever I, Keese CR (1984) Proc Natl Acad Sci USA 81:3761
46. Wegener J, Keese CR, Giaever I (2000) Exp Cell Res 259:158
47. Frisch T, Thoumine O (2002) J Biomech 35:1137
48. Giaever I, Keese CR (1991) Proc Natl Acad Sci USA 88:7896
49. Lo CM, Keese CR, Giaever I (1993) Exp Cell Res 204:102
50. Keese CR, Wegener J, Walker SR, Giaever L (2004) Proc Natl Acad Sci USA 101:1554
51. Schuhmacher R (1990) Angew Chem 102:347
52. Buttry DA, Ward MD (1992) Chem Rev 92:1355
53. Kipling AL, Thompson M (1990) Anal Chem 62:1514
54. Yang MS, Thompson M (1993) Anal Chem 65:1158
55. Sauerbrey G (1959) Zeitschrift Fur Physik 155:206
56. Gryte DM, Ward MD, Hu WS (1993) Biotechnol Progr 9:105
57. Redepenning J, Schlesinger TK, Mechalke EJ, Puleo DA, Bizios R (1993) Anal Chem 65:3378
58. Wegener J, Janshoff A, Galla HJ (1998) Eur Biophys J Biophys Lett 28:26
59. Kanazawa KK, Gordon JG (1985) Anal Chem 57:1770
60. Janshoff A, Wegener J, Sieber G, Galla HJ (1996) Eur Biophys J 25:93

61. Rodahl M, Hook F, Fredriksson C, Keller CA, Krozer A, Brzezinski P, Voinova M, Kasemo B (1997) Faraday Discuss:229
62. Rodahl M, Kasemo B (1996) Rev Sci Instrum 67:3238
63. Fredriksson C, Kihlman S, Rodahl M, Kasemo B (1998) Langmuir 14:248
64. Nimeri G, Fredriksson C, Elwing H, Liu L, Rodahl M, Kasemo B (1998) Colloids Surf B-Biointerfaces 11:255
65. Reiss B, Janshoff A, Steinem C, Seebach J, Wegener J (2003) Langmuir 19:1816
66. Wegener J, Seebach J, Janshoff A, Galla HJ (2000) Biophys J 78:2821
67. Reiß B (2004) Westfälische Wihelms-Universität, Münster
68. Mitchell SA, Poulsson AHC, Davidson MR, Bradley RH (2005) Colloids Surf B-Biointerfaces 46:108
69. Mitchell SA, Poulsson AHC, Davidson MR, Emmison N, Shard AG, Bradley RH (2004) Biomaterials 25:4079
70. Welle A, Gottwald E (2002) Biomed Microdevices 4:33
71. Heitmann V, Wegener J (2007) Anal Chem 79:3392